

1 **Within-patient evolution of plasmid-mediated antimicrobial resistance**

2 Javier DelaFuente^{1,*}, Laura Toribio-Celestino¹, Alfonso Santos-Lopez^{1,2,3}, Ricardo
3 Leon-Sampedro^{2,3,4}, Aida Alonso-del Valle¹, Coloma Costas¹, Marta Hernandez-
4 Garcia^{2,6}, Lun Cui⁵, Jeronimo Rodriguez-Beltran^{2,6}, David Bikard⁵, Rafael Canton^{2,6},
5 Alvaro San Millan^{1,3,*}

6

7 **Author affiliations**

8

9 1. Centro Nacional de Biotecnologia (CNB), CSIC. Madrid, Spain.

10 2. Servicio de Microbiologia. Hospital Universitario Ramon y Cajal-IRYCIS.
11 Madrid, Spain.

12 3. Centro de Investigacion Biologica en Red de Epidemiologia y Salud Pública
13 (CIBERESP), Instituto de Salud Carlos III, Madrid, Spain

14 4. Institute of Integrative Biology, Department of Environmental Systems Science,
15 ETH Zurich, Switzerland

16 5. Institut Pasteur, Universite de Paris, CNRS UMR 6047, Synthetic Biology,
17 75015 Paris, France

18 6. Centro de Investigacion Biologica en Red de Enfermedades Infecciosas
19 (CIBERINFEC), Instituto de Salud Carlos III, Madrid, Spain

20

21 * **Correspondence and request for materials** should be addressed to Javier
22 DelaFuente (fuentehidalgo91@gmail.com) & Alvaro San Millan
23 (asanmillan@cnb.csic.es).

24 **Abstract**

25

26 Antibiotic resistance (AMR) in bacteria is a major threat to public health, and one
27 of the key elements in the spread and evolution of AMR in clinical pathogens is
28 the transfer of conjugative plasmids. The drivers of AMR evolution have been
29 extensively studied *in vitro*, but the evolution of plasmid-mediated AMR *in vivo*
30 remains poorly explored. Here, we tracked the evolution of the clinically-relevant
31 plasmid pOXA-48, which confers resistance to the last-resort antibiotics
32 carbapenems, in a large collection of enterobacterial clones isolated from the gut
33 of hospitalised patients. Combining genomic and experimental approaches, we
34 first characterized plasmid diversity and the genotypic and phenotypic effects of
35 multiple plasmid mutations on a common genetic background. Second, using
36 cutting-edge genomic editing in wild-type multidrug resistant enterobacteria, we
37 dissected three cases of within-patient plasmid-mediated AMR evolution. Our
38 results revealed, for the first time, compensatory evolution of plasmid-associated
39 fitness cost, as well as the evolution of enhanced plasmid-mediated AMR, in
40 bacteria evolving within the gut of hospitalised patients. Crucially, we observed
41 that the evolution of plasmid-mediated AMR *in vivo* involves a pivotal trade-off
42 between resistance levels and bacterial fitness. This study highlights the need to
43 develop new evolution-informed approaches to tackle plasmid-mediated AMR
44 dissemination.

45 **Introduction**

46

47 Antimicrobial resistance (AMR) in bacteria has emerged as a major global threat
48 to public health¹. AMR is particularly concerning in clinical settings, where
49 nosocomial infections increase mortality rates among hospitalised patients and
50 raise the costs associated with infection control and management². The gut
51 microbiota of patients is one of the most important hotspots of AMR dissemination
52 and evolution³, and a crucial element in this process is the transfer of conjugative
53 plasmids – circular DNA molecules that replicate independently of the bacterial
54 chromosome and can transfer horizontally between bacteria⁴.

55 Numerous studies in recent years have characterized the evolution of plasmid-
56 mediated AMR, expanding our understanding of how AMR plasmids evolve and
57 persist in bacterial populations. AMR plasmids dramatically enhance bacterial
58 fitness in the presence of antibiotics, and plasmid-mediated resistance can
59 further evolve through changes in plasmid copy number (PCN)^{5–7}, mutations or
60 duplications of plasmid-encoded AMR genes^{8,9} or interactions with chromosomal
61 mutations¹⁰. However, in the absence of antibiotics, plasmid-induced
62 physiological alterations frequently lead to a decrease in bacterial fitness, a
63 phenomenon known as plasmid cost^{11,12}. This cost can be mitigated over time
64 through compensatory mutations in the plasmid or chromosome^{13–15}.
65 Remarkably, previous studies showed that the costs associated with AMR
66 plasmids mainly arise from the expression of resistance genes^{11,16,17}. This insight
67 suggests that bacteria carrying AMR plasmids probably experience a trade-off
68 between fitness in the presence and absence of antibiotics (fitness-resistance
69 trade-off)^{18,19}. Despite the importance of these earlier studies, current
70 understanding of the evolution of plasmid-mediated resistance derives almost
71 entirely from highly controlled experiments conducted *in vitro*. The lack of access
72 to suitable bacterial collections of clinical origin, together with the arduousness of
73 performing genetic manipulations with wild-type, multidrug-resistant bacterial
74 isolates, has prevented study of the evolution of plasmid-mediated AMR in
75 clinically relevant real-life scenarios.

76 Here, we tracked the evolutionary dynamics of plasmid-mediated AMR in the gut
77 microbiota of hospitalised patients. We focused on the widespread pOXA-48-like
78 conjugative plasmids, which constitute one of the most relevant plasmid groups

79 in clinical settings in Europe^{20,21}. pOXA-48-like plasmids are found in the order
80 *Enterobacterales*, giving rise to carbapenem-resistant enterobacteria, which were
81 recently reported to be the fastest-growing resistance threat in Europe²². We
82 used a previously characterized collection of 224 pOXA-48-carrying
83 enterobacteria isolated over a two-year period from more than 9,000 hospitalised
84 patients at the Ramon y Cajal University Hospital in Madrid, Spain (R-GNOSIS
85 collection, Supp. Fig. 1. For the characterization of pOXA-48-carrying isolates in
86 R-GNOSIS, see^{23–25}). We studied multiple pOXA-48 variants carrying distinct
87 mutations and elucidated the evolution of specific associations between pOXA-
88 48 and wild-type enterobacteria in the gut microbiota of three patients. Our results
89 revealed that the *in vivo* evolution of plasmid-mediated resistance is shaped by
90 interplay between AMR and plasmid-induced fitness costs.

91

92 **Results**

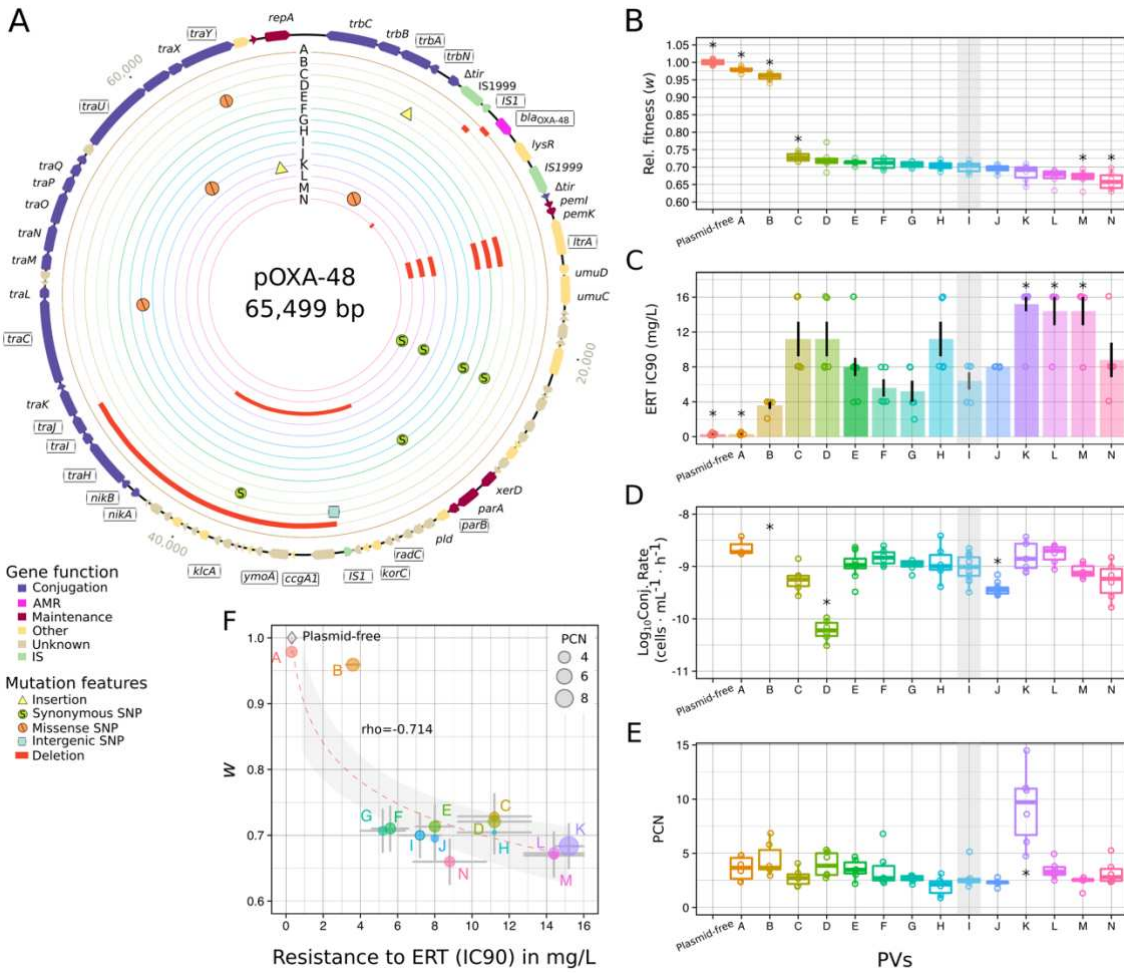
93

94 *Analysis of pOXA-48 plasmid variants*

95 To identify mutations potentially associated with plasmid-mediated AMR
96 evolution, we characterized the genomes of all pOXA-48-like plasmids in the R-
97 GNOSIS collection. Comparison of the full sequences of all 224 pOXA-48-like
98 plasmids, identified a total of 35 plasmid variants (PVs), defined as pOXA-48-like
99 plasmids carrying any SNP or insertion/deletion (indel) compared with the most
100 common variant (PV-I), which is present in ~67% of the isolates in the collection
101 (Figure 1, Supp. Fig.1, Supp. Table 1 and Methods).

102 We next studied the phenotypic and genotypic effects of a selection of 14 of the
103 PVs (Figure 1A and see Methods for PV selection criteria). The 14 pOXA-48
104 variants were introduced into the *Escherichia coli* J53 strain²⁶ (K12 derivative),
105 used as a common isogenic bacterial host to specifically dissect plasmid effects.
106 PVs-carrying J53 genomes were resequenced to confirm plasmid presence and
107 the isogenic nature of the transconjugants (Supp. Table 2, see Methods). The
108 following phenotypic and genotypic variables were examined in each
109 transconjugant and in plasmid-free J53: i) bacterial fitness, assessed from growth
110 curves and competition assays; ii) plasmid conjugation rate; iii) antimicrobial
111 resistance; and iv) plasmid copy number (PCN).

112 The PVs produced a variety of phenotypes in J53 (Figure 1 B-E and Supp. Fig.
113 2). For example, although the fitness effect of most PVs was similar to that of PV-
114 I (the most common PV), two PVs were associated with a large decrease in cost
115 (Kruskal-Wallis rank-sum test, followed by pairwise comparison Wilcoxon rank-
116 sum exact test with FDR correction $P<0.01$). One of these variants (PV-A) had a
117 deletion in the carbapenemase gene *bla*_{OXA-48} that abolished plasmid-mediated
118 AMR (Figure 1C). The other one (PV-B) carried two deletions: i) a small deletion
119 affecting the IS1 element upstream of *bla*_{OXA-48} and ii) a ~13.5 kb deletion
120 including genes involved in conjugation, associated with a conjugation-
121 incompetent phenotype (Figure 1D). PV-D and PV-J both had a lower conjugation
122 rate than PV-I (Figure 1D; Kruskal-Wallis rank-sum test followed by pairwise
123 comparison Wilcoxon rank-sum exact test with FDR correction $P<0.001$) and
124 carried mutations in conjugation-related genes: a nonsynonymous SNP in *traY*
125 and an insertion in *trbN* (PV-D), and a nonsynonymous SNP in *traU* (PV-J) (Supp.
126 Table 1). PCN was significantly elevated in one PV, PV-K (Figure 1E), which
127 carried a mutation upstream of the gene encoding the replication initiation protein
128 RepA (Kruskal-Wallis rank-sum test, followed by pairwise comparison Wilcoxon
129 rank-sum exact test with FDR correction $P=0.022$).
130 Analysis of the effects of AMR, PCN and conjugation rates on plasmid-
131 associated fitness costs in J53 revealed a clear trade-off between AMR and
132 fitness costs (Figure 1F, Spearman's rank correlation $S= 779.7$, $\rho = -0.7136$, $P=$
133 0.004). PVs conferring AMR were associated with a high fitness cost (27%-34%
134 reduction in relative fitness), whereas the two PVs which conferred low or no AMR
135 imposed only a small fitness cost (<4 % reduction in relative fitness). Neither
136 conjugation nor PCN showed a significant association with plasmid fitness costs
137 (Spearman's rank correlation, $P>0.25$, Supp. Fig. 3).



138

139 **Figure 1. pOXA-48 plasmid variants tested in *E. coli* J53.**

140 A) Representation of pOXA-48 variants (PVs) A-N in concentric circles (for variant details see
141 legend). The gene map in the outer circle represents the most common variant (PV-I, used as a
142 reference and highlighted by grey shading in panels B-E). Arrows indicate the reading frames,
143 and colours indicate gene functional classification. Gene names are indicated in the outer circle,
144 and the names of genes showing mutations are represented inside boxes. B) Box plots showing
145 relative fitness (w) of pOXA-48-carrying *E. coli* J53 relative to plasmid-free J53. Horizontal lines
146 inside boxes indicate median values, the upper and lower hinges correspond to the 25th and 75th
147 percentiles, and whiskers extend to observations within the 1.5 \times the interquartile range (IQR).
148 Individual points show independent replicates ($n=6$). C) Resistance to ertapenem (ERT) in
149 plasmid-free and plasmid-carrying *E. coli* J53, represented as the 90% inhibitory concentration
150 (IC90) in mg/L. Bars indicate the mean values and dots indicate individual replicates ($n=10$ for
151 PV-K & PV-E and $n=5$ for the remaining PVs). Black bars represent the standard error of the
152 mean. D) Conjugation rates of different PVs in *E. coli* J53 (in log₁₀ scale, $n=14$ for PV-I, $n=9$ for
153 PV-J, $n=8$ for PV-E & PV-K, $n=3$ for PV-A, and $n=6$ for the remaining PVs), represented as
154 boxplots as in B. E) Plasmid copy number of different PVs in *E. coli* J53, represented as boxplots
155 as in B ($n=6$). Asterisks in panels B-E indicate significance ($P < 0.05$) for the comparison of each
156 PV with PV-I. F) Correlation between relative fitness (w) and resistance to ertapenem (mean IC90)
157 in PV-carrying *E. coli* J53. Individual points indicate the mean value, and lines represent the

158 standard error of the mean IC90 and the propagated standard error of the relative fitness. The
159 size of each point is proportional to PCN in J53. The diamond represents the plasmid-free J53
160 values, which were not included in the correlation. Individual PVs are indicated by letters. The red
161 dashed line indicates the linear regression and the gray-shaded zone covers the 95% confidence
162 interval.

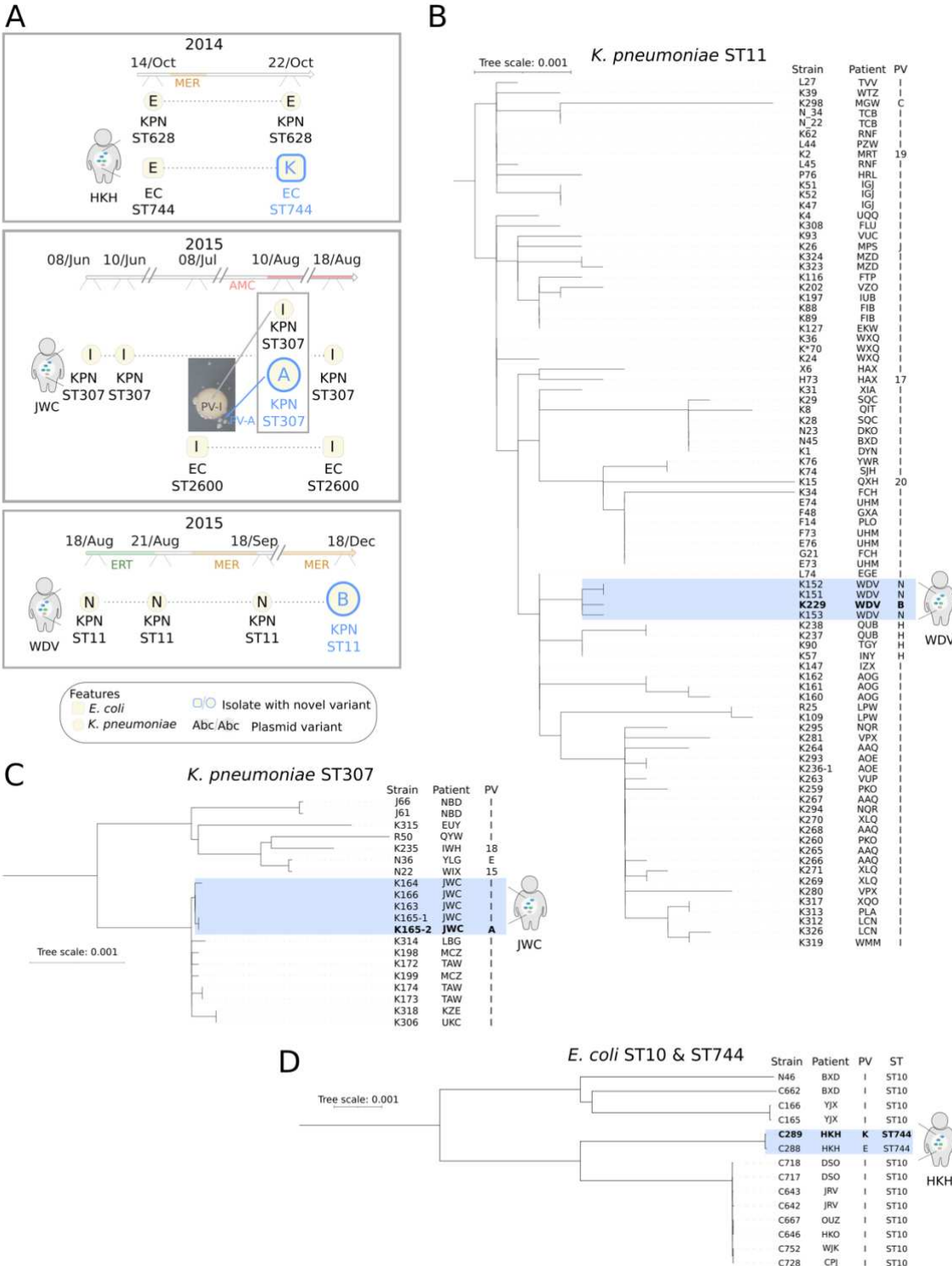
163

164 *Screening within-patient pOXA-48 evolution*

165 The above characterization of pOXA-48 variants suggested that PV mutations,
166 and the resulting fitness-resistance trade-off, could contribute to the evolution of
167 pOXA-48-mediated AMR *in vivo*. In the R-GNOSIS project, hospitalised patients
168 colonized with carbapenemase-producing enterobacteria were sampled
169 periodically, generating timelines of isolates that allowed us now to investigate
170 the evolution of pOXA-48-mediated resistance in the gut of these patients. We
171 screened the timeline of bacterial isolates collected from individual patients and
172 selected isolates from the same clonal background but carrying different PVs,
173 which would suggest within-patient plasmid evolution. Among the 121 patients
174 colonized by pOXA-48-carrying enterobacteria, we identified three whose
175 timelines matched these conditions: patients HKH, JWC, and WDV (Figure 2, see
176 methods).

177 In the genomic analysis of pOXA-48-carrying bacteria from the R-GNOSIS
178 collection, two lines of evidence strongly suggested that plasmid mutations
179 emerged and were subsequently selected in specific clones in the gut microbiota
180 of these three patients. First, comparison of the core genomes of all *K.*
181 *pneumoniae* and *E. coli* isolates revealed a tight grouping of isolates potentially
182 involved in the potential within-patient evolution events (Figure 2B-D, <5 SNPs
183 between all isolates for each clonal line, Supp. Table 3). This result makes it very
184 unlikely that the observations in patients HKH, JWC, and WDV were the result of
185 independent colonization by clones carrying different PVs. Second, each of the
186 novel PVs originating in these patients was restricted to an individual patient, and
187 was not described in any other isolate in the collection (not even in other clones
188 from the same patient). This result challenges the possibility that these new
189 bacteria-PVs associations were generated by independent conjugation events.

190



191

192 **Figure 2. Screening the within-patient evolution of pOXA-48-mediated AMR.**

193 A) Timelines of the isolation of pOXA-48-carrying enterobacteria from patients HKH, JWC, and
194 WDV (see legend). Isolate features are detailed in the legend. Swab dates are indicated next to
195 the timeline (day/month). pOXA-48-selecting antibiotic treatments are indicated in the timeline
196 (MER, meropenem; ERT, ertapenem; AMC, amoxicillin + clavulanic acid). Each PVs is indicated
197 by a letter. Species are indicated by letters and symbols (KPN and circle for *K. pneumoniae*; EC
198 and square for *E. coli*). The multilocus sequence-type code is indicated next to the species label.

199 Isolates in which the new PV was detected are indicated by blue type and larger size. The patient
200 JWC timeline reveals the emergence of two *K. pneumoniae* isolates co-isolated on an agar plate
201 supplemented with ertapenem 0.3 mg/L. B-D) Genetic relationship built using core-genome
202 comparisons (midpoint rooted phylogenetic trees) of *K. pneumoniae* ST11 (n=85, B), *K.*
203 *pneumoniae* ST307 (n=20, C), and *E. coli* ST10 and ST744 (n=12 & n=2 respectively, D) from
204 the collection. Strain designation, patient codes, and PVs are indicated (see Supp table 1).
205 Isolates involved in putative cases of within-patient evolution are highlighted in blue. Bold lettering
206 marks the isolate in which the novel variant was identified. The tree-scale indicates nucleotide
207 substitution per site.

208

209 *Evolution of pOXA-48-mediated resistance in vivo*

210 To characterize the within-patient plasmid-mediated AMR evolution, we studied
211 the isolates carrying the novel PVs in each patient (from now on, identified with
212 the patient code followed by an asterisk, Figure 3A). First, we cured the pOXA-
213 48 PVs from these isolates using an in-house CRISPR-Cas9 system specifically
214 designed to remove plasmids from multidrug-resistant enterobacteria (see
215 methods and Supp. Fig. 4). Then, for each patient, we independently re-
216 introduced both the ancestral PV (the initial PV present in the same clonal line in
217 the same patient) and the novel PVs in these isolates. Crucially, we sequenced
218 the genomes of the wild-type clones by combining long-read and short-read
219 technologies, and resequenced the genomes of all strains after plasmid curing to
220 ensure that no significant mutations occurred during the process (Figure 3A,
221 Supp. Fig. 4 & Supp. Table 3). Once we had introduced the two PVs into each
222 clone, we measured i) plasmid fitness effects, ii) antimicrobial resistance (to all
223 beta-lactam antibiotics used for treatment in these patients), and iii) PCN for
224 every clone (Fig. 3 B-D, Supp. Fig. 4). The results of these analyses are
225 presented in the following sections patient-by-patient in chronological order.

226

227 *Patient HKH. Increased PCN leading to increases in AMR and fitness costs*

228 Four pOXA-48-carrying isolates were recovered from this patient (Figure 2A).
229 Two isolates belonged to a *K. pneumoniae* sequence-type 628 (ST628) clone,
230 and both carried the same plasmid variant (PV-E). The other two isolates
231 belonged to a *Escherichia coli* ST744 clone. The first of the *E. coli* isolates also
232 carried PV-E, while the second (HKH*) was recovered 8 days later and carried a
233 different plasmid variant, PV-K, differing from PV-E by only a single base pair

234 insertion upstream of *repA*. The *in vitro* genotypic characterization in *E. coli* J53
235 had revealed an association between PV-K and increased PCN (Figure 1E).
236 Analysis of the effects of PV-E and PV-K in HKH* revealed that PV-K was present
237 at a higher PCN (from 3 to 8 copies, one-way ANOVA $F=61.42$, d.f.=1,
238 $P_{adj}<0.001$). The high PCN of PV-K in HKH* was associated with increased AMR
239 to ertapenem (Wilcoxon rank-sum test $W=2$, $P=0.02$) and meropenem (Supp. Fig.
240 5 A-B) but decreased fitness in the absence of antibiotics (Wilcoxon rank-sum
241 exact test, $W=306$, $P<0.001$, Fig. 2 B-D, Supp. Fig. 5A-B). Patient HKH's clinical
242 history revealed meropenem treatment before the isolation of HKH*, which
243 carried the high-PCN PV-K.

244

245 *Patient JWC. Loss of AMR leading to amelioration of plasmid cost*

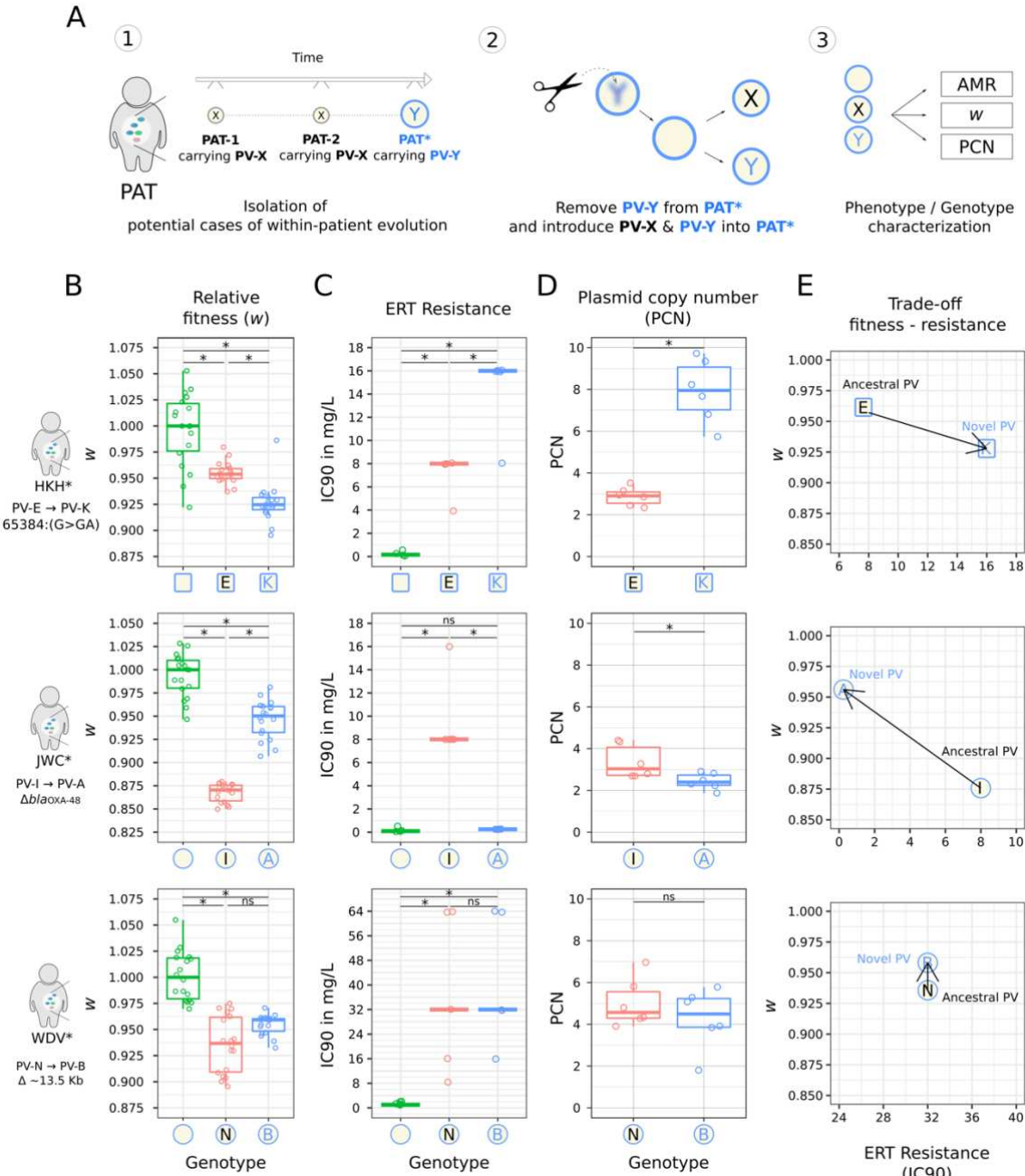
246 Over a 10-week period, six pOXA-48-carrying isolates were recovered from
247 patient JWC (Figure 2A). Four of them belonged to a *K. pneumoniae* ST307 clone
248 and the remaining two to an *E. coli* ST2600 clone. Five isolates carried the most
249 common pOXA-48 variant, PV-I, but the *K. pneumoniae* isolate JWC* carried PV-
250 A, which differs from PV-I by a 199 bp deletion starting 163 bp upstream the
251 coding DNA sequence of the *blaOXA-48* gene. As in the J53 analysis, PV-A was
252 associated not only with loss of resistance to ertapenem and amoxicillin-
253 clavulanic acid in JWC* (Fig. 3C and Supp. Fig. 5 C-D), but also with a reduction
254 in plasmid fitness costs compared with PV-I (Wilcoxon rank-sum test $W=0$,
255 $P<0.001$ for both phenotypes). PV-A was also associated with a modest but
256 significant decrease in PCN in JWC* (one-way ANOVA $F=6.51$, d.f.= 1,
257 $P_{adj}=0.029$, Fig 3 B-D).

258 In R-GNOSIS, carbapenemase-producing enterobacteria were recovered by
259 selective plating, and it was therefore difficult to understand how the carbapenem-
260 susceptible JWC* isolate was obtained from this patient. To investigate this, we
261 plated the original frozen JWC isolate stocks on agar with and without ertapenem.
262 Antibiotic-containing plates inoculated with the JWC* frozen stock (but not the
263 other isolates) contained large resistant colonies of *K. pneumoniae* ST307/PV-I
264 surrounded by smaller susceptible colonies of isogenic *K. pneumoniae*
265 ST307/PV-A (Figure 2A), an example of the phenomenon of cross-protection by
266 secreted beta-lactamases known as satellitism²⁷. Sequencing of the entire
267 genomes of three large and three satellites colonies confirmed that they were

268 isogenic *bla*_{OXA-48+} and *bla*_{OXA-48-} variants of the same *K. pneumoniae* ST307
269 clone. This results strongly suggests that two versions of the *K. pneumoniae*
270 ST307 clone, with the different PVs, coexisted in the patient's gut at that
271 timepoint. Although PV-A and PV-I carrying bacteria coexisted at the time of
272 JWC* sampling (Figure 2A), 8 days later only the fully resistant PV-I-carrying
273 clone was detected. This shift is probably explained by an AMC treatment that
274 began right before the isolation of JWC*, since OXA-48 confers high-level
275 resistance to AMC.

276

277 *Patient WDV. Large plasmid deletion leading to loss of conjugation ability*
278 Four isolates of a *K. pneumoniae* ST11 clone were recovered from this patient
279 over a four-month period. The three initial isolates carried PV-N, but the last
280 isolate (WDV*) carried PV-B, which differed from PV-N by a ~13.5 kb deletion
281 (Figure 2A and Figure 1A). Compared with PV-I, both PV-N and PV-B carry the
282 same small deletion affecting the IS1 element upstream of *bla*_{OXA-48}. The large
283 ~13.5 kb deletion in PV-B affected multiple genes involved in conjugation, leading
284 to the loss of conjugation ability in J53 (Fig. 1). In the wild-type strain, PV-B was
285 also associated with a conjugation-incompetent phenotype, and it produced a
286 small, marginally significant, decrease in fitness costs in WDV* compared with
287 PV-N (Wilcoxon rank-sum exact test $W=101$, $P=0.054$). AMR and PCN were the
288 same in the PV-N-carrying and the PV-B-carrying WDV* isolate (Wilcoxon rank-
289 sum test $W=23$ & $W=14.5$, $P>0.5$). The results from patient WDV thus revealed
290 no clear change in plasmid-associated effects, although the slight difference in
291 fitness costs imposed by PV-N and PV-B could suggest that the large deletion
292 in PV-B might act as a compensatory mutation (Figure 3 B-C and Supp. Fig. 5 E-
293 F).



294

295 **Figure 3. Characterization of the *in vivo* evolution of plasmid-mediated AMR.**

296 A) Workflow used to investigate the within-patient evolution of pOXA-48-mediated AMR. B)
297 B) Relative fitness (*w*) of each plasmid-bacteria combination compared with the plasmid-free strain
298 (see methods). Horizontal lines inside boxes indicate median values, the upper and lower hinges
299 correspond to the 25th and 75th percentiles, and whiskers extend to observations within $1.5 \times$ the
300 IQR. Individual points represent independent replicates ($n=18$). Asterisks in panels B-D indicate
301 significant differences ($P<0.05$ in pairwise comparison Wilcoxon rank-sum exact test with FDR
302 correction in B and C, and $P_{adj}<0.05$ by one-way ANOVA in D); ns, nonsignificant ($P_{adj}>0.05$).
303 C) Resistance to ertapenem (ERT) measured as IC90 (mg/L) of plasmid-free and plasmid-
304 carrying combinations. Lines indicate median values and individual replicates are indicated by
305 points ($n=5$). D) Plasmid copy number (PCN) of each PV, represented in boxplots as in B ($n=6$).
306 E) Schematic representations of the trade-off between antibiotic resistance (median IC90) and

307 relative fitness (median w) in the strains under study. Black arrows represent the trade-off and
308 arrowheads indicate the PVs timeline (from ancestral to novel PV).

309

310 *A fitness-resistance trade-off shapes within-patient evolution of pOXA-48*

311 In line with our observations in *E. coli* J53, the analysis of the *in vivo* evolution of
312 pOXA-48-mediated AMR in patient gut microbiota indicated that this process is
313 shaped by a fitness-resistance trade-off (Figure 3E). Moreover, clinical metadata
314 from patients strongly suggests that antibiotic treatments direct the rapid, and
315 even bidirectional, navigation of this trade-off.

316 In patient JWC we detected coexistence of almost isogenic *K. pneumoniae*
317 ST307 populations differing only in the presence of an intact *bla*_{OXA-48} gene in
318 pOXA-48. The presence of the *bla*_{OXA-48} was associated with fitness cost in the
319 absence of antibiotics. The emergence of the *bla*_{OXA-48}-lacking PV-A followed a
320 two-month period of no OXA-48-selecting antibiotic treatment, but this variant
321 was rapidly depleted by a cycle of amoxicillin + clavulanic acid. This result not
322 only supports the impact of the fitness-resistance trade-off on the evolution of
323 AMR, but also highlights the importance of clonal diversification in the gut
324 microbiota for this process.

325 In patient HKH, meropenem treatment triggered the rapid emergence (8 days
326 between isolates) of PV-K, which conferred increased PCN and AMR. Fitness
327 results indicated that PV-K was associated with an increased fitness cost in the
328 absence of antibiotics. Unfortunately, no further samples from this patient were
329 included in the R-GNOSIS collection, and we were therefore unable to investigate
330 the fate of PV-K after the antibiotic treatment ended.

331

332 **Discussion**

333

334 The role of fitness-resistance trade-offs in the evolution of AMR has received
335 considerable attention^{18,28}. However, despite plasmids being arguably the most
336 important vehicle for the acquisition of clinically relevant AMR in many key
337 pathogens, there was previously little published evidence of the impact of this
338 trade-off on the evolution of plasmid-mediated AMR in clinically relevant
339 situations¹⁹. We anticipate that the fitness-resistance trade-off described here will
340 affect the evolution of plasmid-mediated AMR more generally, because AMR

341 gene expression is one of the central sources of plasmid-associated fitness
342 costs^{11,16,17}. One naive prediction arising from this result is that, in the absence
343 of antibiotic pressure, natural selection could favour plasmid loss or mutations
344 that inactivate plasmid-encoded resistance genes, reversing AMR evolution.
345 However, this prediction is challenged by at least two lines of evidence. First, we
346 observed that the standing genetic variation in the gut microbiota helps to bypass
347 this fitness-resistance trade-off by supporting the coexistence of subpopulations
348 carrying either low-cost/low-resistance or high-cost/high-resistance PVs. Indeed,
349 because of the sampling and isolation protocol used in R-GNOSIS (isolation of
350 one clone per species and time point), the role of preexisting genetic diversity in
351 AMR evolution is probably vastly underestimated in our analysis. Second, we
352 previously reported that pOXA-48 conjugation is pervasive in hospitalised
353 patients and leads to long-term plasmid carriage in their gut²³. In that study, we
354 described an *in vivo* pOXA-48 conjugation event in patient HKH involving the
355 same *E. coli* clone in which we have now described subsequent plasmid
356 evolution. The plasmid dynamics described in this patient perfectly exemplify the
357 ability of pOXA-48 to spread rapidly and to evolve in the gut microbiota of
358 hospitalised patients. The high pOXA-48 conjugation rate will feed the microbiota
359 with a constant supply of new plasmid-carrying bacteria, promoting plasmid
360 maintenance in the bacterial community. These results highlight the need to
361 consider AMR ecology and evolution in order to develop more rational strategies
362 to counteract AMR in complex bacterial communities, such as the gut microbiota.
363 Our study also highlights the need to consider two previously neglected issues in
364 the study of AMR evolution. The first of these is the importance of analysing AMR
365 evolution directly in the wild-type, clinically relevant bacterial strains. Our results
366 showed that although the laboratory *E. coli* strain J53 provides reasonably good
367 qualitative predictions of PVs effects, plasmid-associated fitness costs tend to be
368 much higher than in the wild-type bacteria. This discrepancy could lead to
369 erroneous predictions about the survival of AMR strains in the gut of patients. The
370 second issue is the importance of considering the preexisting genetic diversity in
371 bacterial communities when assessing the potential for AMR evolution. Our
372 results from patient JWC, together with findings from other recent studies^{24,29,30},
373 show that genetic diversity fuels AMR evolution. Most research to date on within-

374 patient evolution of AMR (including this study) has failed properly to screen for
375 community diversity. In future studies, addressing these issues will produce more
376 accurate predictions and help to develop better intervention strategies against
377 AMR in clinical settings.

378

379 **Methods**

380

381 *Bacterial strains, and culture conditions*

382 All experiments were performed in Lennox lysogeny broth (LB) which was -when
383 indicated- supplemented with 15 g/L agar (CONDA, Spain). Mueller Hinton II
384 broth (Oxoid) was used for IC90 determination and results were comparable with
385 those obtained in LB. Amoxicillin+clavulanic acid (Sandoz, Spain), meropenem
386 (Aurovitae, Spain), kanamycin, ertapenem, chloramphenicol, apramycin,
387 streptomycin, sodium azide and carbenicillin (Merck, Spain) were used in this
388 study. Clinical strains used in this study were isolated during the R-GNOSIS
389 project which included 28,089 samples from 9,275 patients in the Hospital
390 Universitario Ramon y Cajal (Madrid, Spain)^{23,25}. For this study only pOXA-48-
391 carrying enterobacteria were included. All primers used in the study are described
392 in Supp. Table 4.

393

394 *Plasmid construction*

395 pBGC²⁴ was used to construct pBGA by exchanging the *cat* gene
396 (chloramphenicol resistance) with *aac(3)-IV* (apracycin resistance) from
397 pMDIAI³¹ by Gibson assembly (New England Biolabs, UK). pLC10-Apra was
398 constructed by exchanging the *aph(3')-la* gene (Kanamycin resistance) with the
399 *aac(3)-IV* gene, by Gibson assembly. Plasmids pLC10-Kan/pLC10-Apra carry the
400 *Streptococcus pyogenes cas9* gene under the control of a Ptet promoter inducible
401 by anhydrotetracycline (derived from pWJ153³²), cloned on a thermosensitive
402 pSC101 plasmid backbone with a guide RNA under the control of a Ptrc promoter
403 derived from pCas³³ (Addgene plasmid #62225). Single guide RNA (sgRNA)
404 targeting pOXA-48 *pemK* gene (Fig.1A) was introduced into pLC10-Kan by
405 golden gate assembly³⁴ (New England Biolabs, UK). pLC10-Apra was
406 constructed by exchanging the *aph(3')-la* gene (Kanamycin resistance) with the
407 *aac(3)-IV* gene, by Gibson assembly.

408

409 *gDNA extraction, short-read (Illumina) and long-read sequencing (MinION)*

410 Genomic DNA was extracted using the Wizard genomic DNA purification kit
411 (Promega). Short-read sequencing data from wild-type strains was obtained from
412 ²³ (BioProject PRJNA626430). Additionally, *E. coli* J53
413 transconjugants/transformants and the wild-type strains involved in within-patient
414 pOXA-48 evolution (K163, K165, C288, C289, K153 and K229) were sequenced
415 in the Microbial Genome Sequencing Center (MIGS, USA) using NextSeq 2000
416 platform (coverage>100x). Long-read sequencing (MinION) was performed in
417 MIGS for the wild-type strains involved in within-patient pOXA-48
418 (coverage>100x). Sequencing data are available under BioProject
419 PRJNA838107. Short-reads from MiGS were trimmed with Trim Galore v0.6.4
420 (<https://github.com/FelixKrueger/TrimGalore>), using a quality threshold of 20 and
421 removing adapters and reads <50 bp. Filtlong v0.2.1
422 (<https://github.com/rrwick/Filtlong>) was used for filtering long-reads.

423

424 *Assembly and analysis of pOXA-48 variants in the enterobacteria collection*

425 R-GNOSIS genomes were assembled as in ²³. pOXA-48_K8 (MT441554) was
426 used as reference in variant calling using Snippy v4.6.0 and plasmids sharing
427 72% of the pOXA-48 core-genome were selected (n=224). Then, nucleotide
428 variants in 48,500-48,853 and 14,883-16,638 zones were discarded. Mutations
429 in 48,500-48,853 were discarded as they were identified by Sanger sequencing
430 (Macrogen, Spain) as false positives during assembly (Illumina data). This zone
431 contains highly repeated nucleotides which Illumina cannot resolve properly. In
432 14,883-16,638 pOXA-48 contained a group-II intron (*ItrA*). *ItrA* sequence was
433 blasted (BLASTn³⁵ v2.11.0) against the assemblies of each strain to confirm its
434 presence/absence in each PVs. Identity differences in *ItrA* sequence were not
435 considered for PVs. Insertions were not detected in hybrid assemblies and were
436 not considered for strains sequenced just with Illumina technology. However, we
437 could manually detect a *bla*_{CTX-M-15} gene insertion in position 7,018 in PV-D, by
438 comparing assemblies and *in vitro* validating by PCR. Deletions between PVs
439 were *in silico* detected with BRIG v0.95³⁶ and validated by PCR amplification. We
440 defined PVs as pOXA-48-like plasmids isolated in R-GNOSIS that share at least

441 a 72% core-genome with pOXA-48_K8 but presented SNPs and/or indels when
442 compared to it.

443

444 *Introducing pOXA-48 variants into bacterial isolates*

445 A subset of 14 PVs was selected for further investigation based on the following
446 criteria: i) PVs carrying non-synonymous mutations/deletions covering a wide
447 representation of different genes and functions and avoiding PVs with redundant
448 mutations in the same genes, ii) PVs carrying insertions and large
449 rearrangements and iii) PVs with intergenic mutations near to housekeeping
450 plasmid genes, such as genes involved in replication, conjugation or partition.
451 Wild-type strains (donors) and *E. coli* J53 (recipient) were streaked from freezer
452 stocks onto solid LB agar with antibiotic selection: ertapenem (0.5 mg/L) and
453 sodium azide (100 mg/L), respectively and incubated overnight at 37°C. Several
454 donor colonies and one recipient colony were independently inoculated in 2 mL
455 of LB in 15-mL tubes and cultured for 6 hours (37°C and 250 rpm, Thermo
456 Scientific™ MaxQ™ 8000). Cultures were centrifuged (15 minutes, 1,500 g) and
457 cells were mixed in 1:2 proportion (donor:recipient) and spotted onto solid LB
458 medium overnight at 37°C. Transconjugants were selected by streaking the mix
459 on LB with ertapenem and sodium azide. The presence of PVs in bacteria was
460 confirmed by Illumina sequencing (MIGS). Additionally, each PVs was validated
461 by PCR amplification and Sanger sequencing. For PV-A, which does not confer
462 AMR, donors and recipients were mixed in 10:1 proportion and transconjugants
463 were selected with sodium azide for *E. coli* J53 or Streptomycin 100 mg/L for the
464 wild-type strain. The presence of the plasmid was confirmed by PCR screening
465 multiple colonies. PV-B was isolated with the NucleoBond Xtra Midi Plus kit
466 (MACHEREY-NAGEL, USA), and introduced into bacteria by electroporation as
467 in ³⁷. Transformants were selected in LB agar with amoxicillin 200 mg/L +
468 clavulanic acid 40mg/L.

469

470 *De novo assembling and genomic analysis of *E. coli* J53 carrying different PVs*

471 Genomes were assembled using SPAdes³⁸ v3.15.2. Assembly quality was
472 assessed with Quast³⁹ v5.0.2. All assemblies reached a size of 4.6-4.8 Mb and
473 contigs >500 bp count was under 110. Prokka⁴⁰ v1.14.6 was used to annotate
474 genomes. Snippy v4.6.0 (<https://github.com/tseemann/snippy>) was used to

475 identify variants in the *E. coli* J53 genome by mapping Illumina reads back to its
476 assembly. Variants in the J53 strains carrying PVs were called with Snippy and
477 breseq⁴¹ v0.35.6 using the annotated *E. coli* J53 genome as reference. Variants
478 matching in J53 were discarded as assembly errors. From breseq output only
479 predicted mutations and unassigned missing coverage (MC) were analysed
480 because of Illumina data limitations. Snippy was used in a reverse approach,
481 mapping the reads of *E. coli* J53 against the assemblies of the PVs-carriers.
482 Unidentified mutations not identified in both comparisons and by both software
483 were discarded. For pOXA-48 analysis Snippy and breseq were run using as
484 reference pOXA-48_K8 (MT441554). Only mutations called by both programs, as
485 well as MC and JC from breseq, were considered. The sequence of the *ltrA* gene
486 was blasted (BLASTn³⁵ v2.11.0) against the assemblies of J53 and the PVs
487 carriers. The contig containing *ltrA* had similar length in all assemblies and
488 different coverage than of chromosomal contigs, indicating that the *ltrA* gene did
489 not move into the chromosome of J53. Plasmid replicons were detected with
490 ABRicate v1.0.1 (<https://github.com/tseemann/abricate>) using the *plasmidfinder*
491 database⁴². *Resfinder* database⁴³ and ABRicate were used to discard the
492 presence of other resistance genes (Supp. Table 2).

493

494 *High throughput relative fitness determination by competition assays*

495 Competition assays were performed by using GFP-tagged strains to distinguish
496 between populations with flow cytometry (CytoFLEX Platform Beckman Coulter
497 Life Sciences, USA). Parameters were: 50 μ l min⁻¹ flow rate, 22 μ m core size,
498 and 10,000 events per well. Competitions were performed by competing each
499 genotype against a GFP-tagged strain. In *E. coli* J53, each genotype had 6
500 replicates and the common competitor was the plasmid-free strain with pBGC²⁴.
501 In clinical strains, competitions were performed by competing each genotype
502 (plasmid-free, and the same strain carrying different PVs against a common
503 competitor). Each genotype was obtained from independent
504 conjugation/transformation events, resulting in 3 independent replicates
505 measured 6 times each (n=18 for each genotype). The common competitor for
506 clinical strains were HKH*/PV-K + pBGA, JWC*/PV-A + pBGC and WDV*/PV-B
507 + pBGA for each case. The common competitors carried PVs to avoid conjugative
508 transfer during competition assays through plasmid exclusion mechanisms⁴⁴.

509 Note that pBGA only differs from pBGC in the AMR gene (apramycin &
510 chloramphenicol resistance respectively). These plasmids contain a *gfp* gene
511 which is under the control of the P_{BAD} promoter, so GFP production is controlled
512 by the presence of L-Arabinose. Pre-cultures were incubated overnight in LB in
513 96-well plates at 250 rpm (Thermo Scientific™ MaxQ™ 8000) 37°C, then mixed
514 1:1 and diluted 400-fold in 200 μ l of fresh LB in 96-well plates (Thermo Scientific,
515 Denmark), and incubated during 24 in the same conditions. The initial populations
516 were mixed (1:1) followed by diluting 400-fold in 200 μ l of NaCl 0.9% with L-
517 arabinose 0.5 % (Sigma, Spain) and incubated at 37 °C at 250 rpm during 1.5
518 hours to induce GFP expression. After 24 hours, final proportions were
519 determined as described above. The fitness of each strain relative to the GFP-
520 tagged one was determined using equation (1):

521

$$(1) w = \frac{\ln\left(\frac{Nf}{Ni}\right)}{\ln\left(\frac{Nf \ gfp}{Ni \ gfp}\right)}$$

522 Where w is the relative fitness of each strain carrying a determined pOXA-48
523 variant compared to the GFP-tagged competitor. Ni and Nf are the number of
524 cells of *gfp*-free clones at the beginning (Ni) and end (Nf) of the competition. Ni
525 gfp and $Nf \ gfp$ are the number of cells of the common GFP-tagged competitor at
526 the beginning and end of the competition respectively. We discarded PVs loss
527 during the competition by growing individually plasmid-carrying bacteria on LB
528 agar and plasmid-selective antibiotics and counting colony forming units per mL
529 at the beginning and end of the assay (PV-A was tested by PCR). Relative fitness
530 (w) was normalised using the w from the common competitors in each case. An
531 underrepresentation of plasmid costs during the competition assay in *E. coli* J53
532 due to conjugative transfer was also discarded by comparing growth curve data
533 (using area under the growth curve, AUC) with relative fitness (Supp. Fig. 2B).

534

535 *Growth curves*

536 Growth curves were performed as in⁴⁵. Briefly, strains were streaked from freezer
537 stocks onto solid LB-agar and incubated overnight at 37°C. The next day single
538 colonies were grown in 2 mL of LB and incubated overnight at 37°C with
539 continuous shaking (250 rpm, Thermo Scientific™ MaxQ™ 8000). Six overnight
540 cultures were diluted 1:1,000 into fresh LB in flat-bottom 96-well plates (Thermo

541 Scientific, Denmark), which were incubated during 24 hours at 37 °C 250 rpm.
542 Optical densities (OD600) were measured every 10 minutes during the incubation
543 in a plate reader (Synergy HTX Multi-Mode Reader, BioTek Instruments, USA).
544 The area under the growth curve (AUC) was determined by using the *growthrates*
545 v0.8.2 & *flux* v0.3-0 packages in *Rstudio* 2021.09.2+382. When determining
546 plasmid-variants cost in *E. coli* J53, normalised AUC was calculated by dividing
547 the AUC of each pOXA-48-carrying isolate by the average value of the AUC of
548 the pOXA-48-free isolate from each plate.

549

550 *Antimicrobial susceptibility testing*

551 Bacterial AMR profile was determined by (i) LB-growth curves in the presence of
552 different antibiotics and (ii) calculation of inhibitory concentration 90 (IC90) which
553 corresponds to the antibiotic concentration inhibiting 90% of the bacterial growth
554 in the absence of antibiotics. For (i) we used the protocol described above and
555 for (ii) strains were streaked from freezer stocks onto solid MH-agar medium and
556 incubated overnight (37°C). Then, single colonies of bacterial cells (n=5 or 10)
557 were inoculated in parallel in liquid MH starter cultures and incubated at 37°C for
558 24 hours at 250 rpm. Later, each culture was diluted 1:1,000 in MH medium (~10⁶
559 cfu) and 200 µl of the final solution were added to a flat-bottom 96-well plate
560 (Thermo Scientific, Denmark) containing the appropriate antibiotic concentration.
561 Antibiotics tested were ertapenem, meropenem and amoxicillin+clavulanic acid.
562 IC90 values were measured after 24 hours of incubation (37°C). Optical density
563 at 600 nm (OD600) was determined in a Synergy HTX (BioTek Instruments, USA)
564 plate reader after 30 seconds of orbital shaking. MH containing each antibiotic
565 concentration was used as blank.

566

567 *Determining plasmid transfer rate in E. coli J53*

568 PVs transfer rate was evaluated using *E. coli* J53 as donor and *E. coli* J53/pBGC
569 (a non-mobilizable and chloramphenicol-resistant plasmid) as recipient. Donors
570 and recipients were streaked in selective agar (ertapenem 0.5mg/L or
571 chloramphenicol 50µg/mL, respectively). After an overnight incubation at 37°C,
572 colonies of each donor and the recipient strain were independently inoculated in
573 2 mL of LB in 15-mL culture tubes and incubated overnight at 37 °C and 250 rpm
574 (Thermo Scientific™ MaxQ™ 8000). Then, 100 µl of donor and recipient were

575 mixed in a 1:1 proportion and incubated on a LB agar plate at 37°C for 2 hours.
576 Subsequently, serial dilutions of each mix were prepared in sterile NaCl 0.9% and
577 plated on selective media for each genotype (carbenicillin 100 µg mL⁻¹,
578 Chloramphenicol 50µg/mL and both antibiotics together). Conjugation rates were
579 determined using the end-point method for solid surfaces as in ²³.

580

581 *Plasmid copy number determination by quantitative PCR (qPCR)*

582 Each genotype was streaked in LB agar and incubated overnight at 37°C. The
583 next day 2 independent colonies were resuspended in 800 µl in sterile water
584 (Fisher Scientific, Spain) and boiled for 10 minutes (95°C). Each sample was
585 centrifuged to spin down cellular debris. Then, 3 independent reactions per
586 colony were performed in triplicate, with 1 µl of the supernatant as DNA template
587 and using with the NZYSupreme qPCR Green Master Mix (2x), ROX plus kit
588 (NZYtech, Portugal) and the 7500 Real Time PCR System (Applied Biosystems,
589 USA). Targeted plasmid and chromosome genes were *bla*_{OXA-48} (amplicon size
590 200 pb; efficiency 97.35-98.09%, r²=0.996-0.986) & *dnaE* (chromosomal gene
591 with one copy, amplicon size 200 bp; efficiency 98.44-100.64%, r²= 0.989-0.996)
592 respectively. The efficiency was calculated using serial 1/4 dilutions of K8 strain
593 (PV-I) and J53/PV-I as in ⁴⁶. The amplification conditions were: 5 minutes
594 denaturation (95°C) followed by 30 cycles of 15 seconds denaturation, 30
595 seconds annealing (55°C) and 30 seconds extension (60°C). The relative plasmid
596 copy number was calculated using equation (2):

$$597 (2) PCN = \frac{(1 + Ec)^{CTc}}{(1 + Ep)^{CTp}}$$

598 where PCN is the plasmid copy number per chromosome, Ec and Ep are the
599 efficiencies of the chromosomal and plasmid reactions (relative to 1), and CTc
600 and CTp are the threshold cycles for chromosomal and plasmid reactions.

601

602 *Curing pOXA-48 like plasmids using a CRISPR/Cas9-based system and*
603 *reintroducing PVs into the clinical isolates*

604 Two different plasmid versions carrying CRISPR/Cas9 machinery were used in
605 this project: pLC10-Kan (kanamycin resistant) and pLC10-Apra (apramycin
606 resistant). pLC10-Kan was used in JWC* and HKH* and pLC10-Apra in WDV*.
607 First pOXA-48 carrying strains were made competent following the protocol

608 described in ³⁶. Then each pLC10 was introduced in the cells by electroporation
609 using 0.1 cm cuvettes and 1.8 kV pulse (MicroPulser Electroporator, Biorad
610 Spain). Transformants were selected on LB agar plates with kanamycin 250-
611 512mg/L or apramycin 30mg/L for each case. Transformants were verified by
612 PCR (Supp. Table 4). Then, CRISPR/Cas9 machinery was induced by
613 resuspending several transformant colonies in 500 μ l of LB with kanamycin or
614 apramycin, 0.2 mg/L anhydrotetracycline (aTc), to activate *Cas9* expression, and
615 IPTG 0.08 mM to enhance sgRNA expression. Then, suspensions were
616 incubated for 2 hours at 30°C with agitation (250 rpm, Thermo Scientific™
617 MaxQ™ 8000) and was streaked and incubated overnight at 37°C on LB agar to
618 cure pLC10. Note that pLC10 *oriC* is based on pSC101 and codes for a
619 thermosensitive replication protein. The next day single colonies were streaked
620 parallelly in LB agar and LB agar supplemented with ertapenem 0.5 mg/L,
621 kanamycin or apramycin. Only colonies that were sensitive to both antibiotics
622 were recovered and sequenced by Illumina (MIGS, USA). Then different plasmid
623 variants were re-introduced in triplicate (in parallel) to plasmid-free cells as
624 described above.

625

626 *Analysis of wild-type strains involved in within-patient pOXA-48 evolution*
627 4 potential cases of within-patient pOXA-48 evolution were identified: HKH, JWC,
628 WDV and HAX. HAX was discarded because the PVs differed from each other
629 just by a synonymous SNP (Supp. Table 1). Unicycler⁴⁷ v0.4.9 with default
630 parameters was used to obtain hybrid-assemblies from K153, K229, C288, C289,
631 K163 and K165 strains. Long-reads were also assembled with Flye⁴⁸ v2.9 and
632 circularization was confirmed in Bandage⁴⁹ v0.8.1. Medaka v1.4.3
633 (<https://github.com/nanoporetech/medaka>) was used to obtain consensus
634 sequences. Several rounds of Pilon⁵⁰ v1.24 were performed mapping the
635 trimmed Illumina reads. Contigs were rotated with Circlator fixstart⁵¹ v1.5.5. Long-
636 read assembly quality was controlled in IGV⁵² v2.11.1. PVs assemblies were
637 confirmed by mapping short- and long-reads and by aligning the assemblies to
638 the reference pOXA-48_K8 (MT441554) with BWA-MEM⁵³ v0.7.17 and
639 minimap2⁵⁴ v2.21. Alignments were visualized in IGV. Closed assemblies were
640 annotated with PGAP⁵⁵ v2021-07-01.build5508. Breseq v0.36.0 was used to
641 identify SNPs and structural variants. To discard false-positive calls different

642 combinations of breseq runs were performed. For K164, K165-2 cured, K165-1,
643 K165-3, K165-4, K165-5, K165-6, K165-7 and K166 (JWC), K151, K152, K229
644 cured (WDV) and C289 cured (HKh), the trimmed reads were mapped to the
645 closed strains from their respective patients. ABRicate v1.0.1 with the
646 *plasmidfinder* and *resfinder* databases was used to confirm clonality and
647 isogeneity between within-patient evolved and cured strains. Further details on
648 workflow and analysis criteria are provided in
649 https://github.com/LaboraTORIbio/within_patient_evolution.

650

651 *Construction of phylogenetic trees*

652 Snippy v4.6.0 was used to find SNPs between all *E. coli* ST10 & ST744
653 (reference C288), *K. pneumoniae* ST11 (reference K153) and *K. pneumoniae*
654 ST307 (reference K163) from the R-GNOSIS collection. Strain K25 (ST11) was
655 removed from the analysis because the fastq files were truncated. Snippy-core
656 (<https://github.com/tseemann/snippy>) was used to find the core genome. Strain
657 K78 (ST11) was removed for diverging too much from the rest of the strains.
658 Gubbins⁵⁶ v3.1.4 was used to remove recombinant regions and SNPs were
659 extracted with snp-sites⁵⁷ v2.5.1. Maximum-likelihood trees were constructed
660 with IQ-TREE⁵⁸ v1.6.12 from the extracted alignments with best evolutionary
661 model detection and an ultrafast bootstrap of 1000 optimized by hill-climbing
662 nearest neighbour interchange (NNI) on the corresponding bootstrap alignment.
663 Trees were visualized and edited in iTOL⁵⁹ and Inkscape v0.17.

664

665 *Statistical analyses*

666 All statistical analyses were performed in *Rstudio* 2021.09.2+382 (R v4.1.1 2021-
667 08-10) with packages *rstatix* v0.7.0, *tidyverse* v1.3.1 and *car* v3.0-12. To test
668 homoscedasticity and the normality of data for each dataset, Shapiro-Wilk test,
669 Levene's Test and Bartlett's test were performed. Then according to each data
670 structure parametric and nonparametric tests were performed (see main
671 manuscript for each test).

672

673 **Acknowledgments**

674

675 We appreciate the technical support of Laura Jaraba Soto. We also thank Craig
676 MacLean, José Penadés, José Antonio Escudero and Daniel Padfield for
677 constructive comments. This work was supported by the European Research
678 Council under the European Union's Horizon 2020 research and innovation
679 programme (ERC grant agreement no. 757440-PLASREVOLUTION) and by the
680 Instituto de Salud Carlos III (PI19/00749) co-funded by European Development
681 Regional Fund 'a way to achieve Europe'. The R-GNOSIS project received
682 financial support from the European Commission (grant no. R-GNOSIS-FP7-
683 HEALTH-F3-2011-282512). A.S.-L. is supported by the European Commission
684 (H2020-MSCA-IF-2019, 895671-REPLAY) and by the European Society of
685 Clinical Microbiology and Infectious Diseases (ESCMID, Research Grant 2022).
686 J.R.-B. acknowledges financial support by a Miguel Servet contract from Instituto
687 de Salud Carlos III (ISCIII) (grant no. CP20/00154), co-funded by ESF, 'Investing
688 in your future', CIBERINFEC, co-funded with FEDER funds, and project
689 PI21/01363, funded by Instituto de Salud Carlos III (ISCIII) and co-funded by the
690 European Union.

691

692 **Author contributions**

693

694 A.S.M and J.DF were responsible for the conceptualization of the study; J.DF,
695 L.C, D.B. and A.S.M designed the methodology. L.T.-C, J.DF and R.L.-S
696 analysed the genomic data; C.C, A.S.-L., A.A.V and J.DF performed experiments
697 and contributed to data analysis; R.C. designed and supervised sampling and
698 collection of bacterial isolates. M.H.-G. collected the bacterial isolates. J.DF and
699 A.S.M analysed data and prepared the original draft of the manuscript and
700 undertook the reviewing and editing; All authors supervised and approved the
701 final version of the manuscript; A.S.M was responsible for funding acquisition and
702 supervision.

703

704 **Data availability**

705

706 The sequence data that support the findings of this study are available in the
707 National Center for Biotechnology Information Database with the accession code

708 PRJNA838107 (<https://www.ncbi.nlm.nih.gov/bioproject/838107>). The remaining
709 R-GNOSIS sequences can be found in ²³.

710

711 **Competing interests**

712

713 The authors declare no competing interests.

714

715

716 **References**

- 717 1. Murray, C. J. *et al.* Global burden of bacterial antimicrobial resistance in 2019: a
718 systematic analysis. *The Lancet* **399**, 629–655 (2022).
- 719 2. Vincent, J.-L. *et al.* International study of the prevalence and outcomes of
720 infection in intensive care units. *JAMA* **302**, 2323–9 (2009).
- 721 3. van Schaik, W. The human gut resistome. *Philosophical Transactions of the*
722 *Royal Society B: Biological Sciences* **370**, 20140087 (2015).
- 723 4. Partridge, S. R., Kwong, S. M., Firth, N. & Jensen, S. O. Mobile Genetic
724 Elements Associated with Antimicrobial Resistance. *Clinical Microbiology*
725 *Reviews* **31**, (2018).
- 726 5. Dimitriu, T., Matthews, A. C. & Buckling, A. Increased copy number couples the
727 evolution of plasmid horizontal transmission and plasmid-encoded antibiotic
728 resistance. *Proceedings of the National Academy of Sciences* **118**, e2107818118
729 (2021).
- 730 6. San Millan, A., Escudero, J. A., Gifford, D. R., Mazel, D. & MacLean, R. C.
731 Multicopy plasmids potentiate the evolution of antibiotic resistance in bacteria.
732 *Nature Ecology & Evolution* **1**, 0010 (2017).
- 733 7. Wheatley, R. *et al.* Rapid evolution and host immunity drive the rise and fall of
734 carbapenem resistance during an acute *Pseudomonas aeruginosa* infection.
735 doi:10.1038/s41467-021-22814-9.
- 736 8. Fröhlich, C. *et al.* Cryptic β -Lactamase Evolution Is Driven by Low β -Lactam
737 Concentrations. *mSphere* **6**, (2021).
- 738 9. Souque, C., Escudero, J. A. & MacLean, R. C. Integron activity accelerates the
739 evolution of antibiotic resistance. *Elife* **10**, (2021).
- 740 10. Bottery, M. J., Wood, A. J. & Brockhurst, M. A. Adaptive modulation of
741 antibiotic resistance through intragenomic coevolution. *Nature Ecology &*
742 *Evolution* **1**, 1364–1369 (2017).
- 743 11. Vogwill, T. & MacLean, R. C. The genetic basis of the fitness costs of
744 antimicrobial resistance: a meta-analysis approach. *Evolutionary Applications* **8**,
745 284–295 (2015).
- 746 12. Martínez-García, L., González-Alba, J. M., Baquero, F., Cantón, R. & Galán, J.
747 C. Ceftazidime Is the Key Diversification and Selection Driver of VIM-Type
748 Carbapenemases. *mBio* **9**, (2018).
- 749 13. Brockhurst, M. A. & Harrison, E. Ecological and evolutionary solutions to the
750 plasmid paradox. *Trends in Microbiology* (2021) doi:10.1016/j.tim.2021.11.001.
- 751 14. Loftie-Eaton, W. *et al.* Compensatory mutations improve general permissiveness
752 to antibiotic resistance plasmids. *Nature Ecology & Evolution* **1**, 1354–1363
753 (2017).
- 754 15. Hall, J. P. J. *et al.* Plasmid fitness costs are caused by specific genetic conflicts
755 enabling resolution by compensatory mutation. *PLoS Biology* **19**, (2021).
- 756 16. Rajer, F. & Sandegren, L. The Role of Antibiotic Resistance Genes in the Fitness
757 Cost of Multiresistance Plasmids. *mBio* **13**, e0355221 (2022).
- 758 17. Humphrey, B. *et al.* Fitness of *Escherichia coli* strains carrying expressed and
759 partially silent IncN and IncP1 plasmids. *BMC Microbiology* **12**, 1–9 (2012).
- 760 18. Andersson, D. I. & Hughes, D. Antibiotic resistance and its cost: Is it possible to
761 reverse resistance? *Nature Reviews Microbiology* vol. 8 260–271 (2010).
- 762 19. Basra, P. *et al.* Fitness Tradeoffs of Antibiotic Resistance in Extraintestinal
763 Pathogenic *Escherichia coli*. *Genome Biology and Evolution* **10**, 667–679 (2018).
- 764 20. Bonomo, R. A. *et al.* Carbapenemase-Producing Organisms: A Global Scourge.
765 *Clinical Infectious Diseases* **66**, 1290–1297 (2018).

766 21. David, S. *et al.* Epidemic of carbapenem-resistant *Klebsiella pneumoniae* in
767 Europe is driven by nosocomial spread. *Nature Microbiology* **4**, 1919–1929
768 (2019).

769 22. Cassini, A. *et al.* Attributable deaths and disability-adjusted life-years caused by
770 infections with antibiotic-resistant bacteria in the EU and the European Economic
771 Area in 2015: a population-level modelling analysis. *The Lancet Infectious
772 Diseases* **19**, 56–66 (2019).

773 23. León-Sampedro, R. *et al.* Pervasive transmission of a carbapenem resistance
774 plasmid in the gut microbiota of hospitalized patients. *Nature Microbiology* **6**,
775 606–616 (2021).

776 24. Alonso-del Valle, A. *et al.* Variability of plasmid fitness effects contributes to
777 plasmid persistence in bacterial communities. *Nature Communications* **12**, 2653
778 (2021).

779 25. Hernández-García, M. *et al.* Characterization of carbapenemase-producing
780 Enterobacteriaceae from colonized patients in a university hospital in Madrid,
781 Spain, during the R-GNOSIS project depicts increased clonal diversity over time
782 with maintenance of high-risk clones. *Journal of Antimicrobial Chemotherapy*
783 **73**, 3039–3043 (2018).

784 26. Matsumura, Y., Peirano, G. & Pitout, J. D. D. Complete Genome Sequence of
785 *Escherichia coli* J53, an Azide-Resistant Laboratory Strain Used for Conjugation
786 Experiments. *Genome Announcements* **6**, (2018).

787 27. Yurtsev, E. A., Chao, H. X., Datta, M. S., Artemova, T. & Gore, J. Bacterial
788 cheating drives the population dynamics of cooperative antibiotic resistance
789 plasmids. *Molecular Systems Biology* **9**, (2013).

790 28. zur Wiesch, P. A., Kouyos, R., Engelstädtter, J., Regoes, R. R. & Bonhoeffer, S.
791 Population biological principles of drug-resistance evolution in infectious
792 diseases. *The Lancet Infectious Diseases* **11**, 236–247 (2011).

793 29. Caballero, J. D. *et al.* Polyclonal pathogen populations accelerate the evolution of
794 antibiotic resistance in patients. (2022) doi:10.1101/2021.12.10.472119.

795 30. Stacy, M. *et al.* Minimizing treatment-induced emergence of antibiotic
796 resistance in bacterial infections. *Science* (1979) **375**, 889–894 (2022).

797 31. Yang, J. *et al.* High-Efficiency Scarless Genetic Modification in *Escherichia coli*
798 by Using Lambda Red Recombination and I-SceI Cleavage. *Applied and
799 Environmental Microbiology* **80**, 3826–3834 (2014).

800 32. Goldberg, G. W., Jiang, W., Bikard, D. & Marraffini, L. A. Conditional tolerance
801 of temperate phages via transcription-dependent CRISPR-Cas targeting. *Nature*
802 **514**, 633 (2014).

803 33. Jiang, Y. *et al.* Multigene Editing in the *Escherichia coli* Genome via the
804 CRISPR-Cas9 System. (2015) doi:10.1128/AEM.04023-14.

805 34. Engler, C., Kandzia, R. & Marillonnet, S. A One Pot, One Step, Precision
806 Cloning Method with High Throughput Capability. *PLOS ONE* **3**, e3647 (2008).

807 35. Altschul, S. F., Gish, W., Miller, W., Myers, E. W. & Lipman, D. J. Basic local
808 alignment search tool. *Journal of Molecular Biology* **215**, 403–410 (1990).

809 36. Alikhan, N. F., Petty, N. K., ben Zakour, N. L. & Beatson, S. A. BLAST Ring
810 Image Generator (BRIG): Simple prokaryote genome comparisons. *BMC
811 Genomics* **12**, 1–10 (2011).

812 37. Fournet-Fayard, S., Joly, B. & Forestier, C. Transformation of wild type
813 *Klebsiella pneumoniae* with plasmid DNA by electroporation. *Journal of
814 Microbiological Methods* **24**, 49–54 (1995).

815 38. Prjibelski, A., Antipov, D., Meleshko, D., Lapidus, A. & Korobeynikov, A.
816 Using SPAdes De Novo Assembler. *Current Protocols in Bioinformatics* **70**,
817 (2020).

818 39. Mikheenko, A., Prjibelski, A., Saveliev, V., Antipov, D. & Gurevich, A.
819 Versatile genome assembly evaluation with QUAST-LG. *Bioinformatics* **34**,
820 i142–i150 (2018).

821 40. Seemann, T. Prokka: rapid prokaryotic genome annotation. *Bioinformatics* **30**,
822 2068–2069 (2014).

823 41. Deatherage, D. E. & Barrick, J. E. Identification of mutations in laboratory
824 evolved microbes from next-generation sequencing data using breseq. *Methods*
825 *Mol Biol* **1151**, 165 (2014).

826 42. Carattoli, A. *et al.* In Silico detection and typing of plasmids using plasmidfinder
827 and plasmid multilocus sequence typing. *Antimicrobial Agents and*
828 *Chemotherapy* **58**, 3895–3903 (2014).

829 43. Zankari, E. *et al.* Identification of acquired antimicrobial resistance genes.
830 *Journal of Antimicrobial Chemotherapy* **67**, 2640–2644 (2012).

831 44. Garcillán-Barcia, M. P. & de la Cruz, F. Why is entry exclusion an essential
832 feature of conjugative plasmids? *Plasmid* **60**, 1–18 (2008).

833 45. DelaFuente, J., Rodriguez-Beltran, J. & San Millan, A. Methods to Study Fitness
834 and Compensatory Adaptation in Plasmid-Carrying Bacteria. *Methods in*
835 *Molecular Biology* **2075**, 371–382 (2020).

836 46. Millan, A. S. *et al.* Small-plasmid-mediated antibiotic resistance is enhanced by
837 increases in plasmid copy number and bacterial fitness. *Antimicrob Agents*
838 *Chemother* **59**, 3335–3341 (2015).

839 47. Wick, R. R., Judd, L. M., Gorrie, C. L. & Holt, K. E. Unicycler: Resolving
840 bacterial genome assemblies from short and long sequencing reads. *PLOS*
841 *Computational Biology* **13**, e1005595 (2017).

842 48. Kolmogorov, M., Yuan, J., Lin, Y. & Pevzner, P. A. Assembly of long, error-
843 prone reads using repeat graphs. *Nature Biotechnology* **2019 37:5** **37**, 540–546
844 (2019).

845 49. Wick, R. R., Schultz, M. B., Zobel, J. & Holt, K. E. Bandage: interactive
846 visualization of de novo genome assemblies. *Bioinformatics* **31**, 3350–3352
847 (2015).

848 50. Walker, B. J. *et al.* Pilon: An Integrated Tool for Comprehensive Microbial
849 Variant Detection and Genome Assembly Improvement. *PLOS ONE* **9**, e112963
850 (2014).

851 51. Hunt, M. *et al.* Circlator: Automated circularization of genome assemblies using
852 long sequencing reads. *Genome Biology* **16**, 1–10 (2015).

853 52. Robinson, J. T. *et al.* Integrative genomics viewer. *Nature Biotechnology* **2011**
854 **29:1** **29**, 24–26 (2011).

855 53. Li, H. & Durbin, R. Fast and accurate long-read alignment with Burrows–
856 Wheeler transform. *Bioinformatics* **26**, 589–595 (2010).

857 54. Li, H. Minimap2: pairwise alignment for nucleotide sequences. *Bioinformatics*
858 **34**, 3094–3100 (2018).

859 55. Tatusova, T. *et al.* NCBI prokaryotic genome annotation pipeline. *Nucleic Acids*
860 *Research* **44**, 6614–6624 (2016).

861 56. Croucher, N. J. *et al.* Rapid phylogenetic analysis of large samples of
862 recombinant bacterial whole genome sequences using Gubbins. *Nucleic Acids*
863 *Research* **43**, e15–e15 (2015).

864 57. Page, A. J. *et al.* SNP-sites: rapid efficient extraction of SNPs from multi-
865 FASTA alignments. *Microb Genom* **2**, e000056 (2016).

866 58. Nguyen, L. T., Schmidt, H. A., von Haeseler, A. & Minh, B. Q. IQ-TREE: A
867 Fast and Effective Stochastic Algorithm for Estimating Maximum-Likelihood
868 Phylogenies. *Molecular Biology and Evolution* **32**, 268–274 (2015).

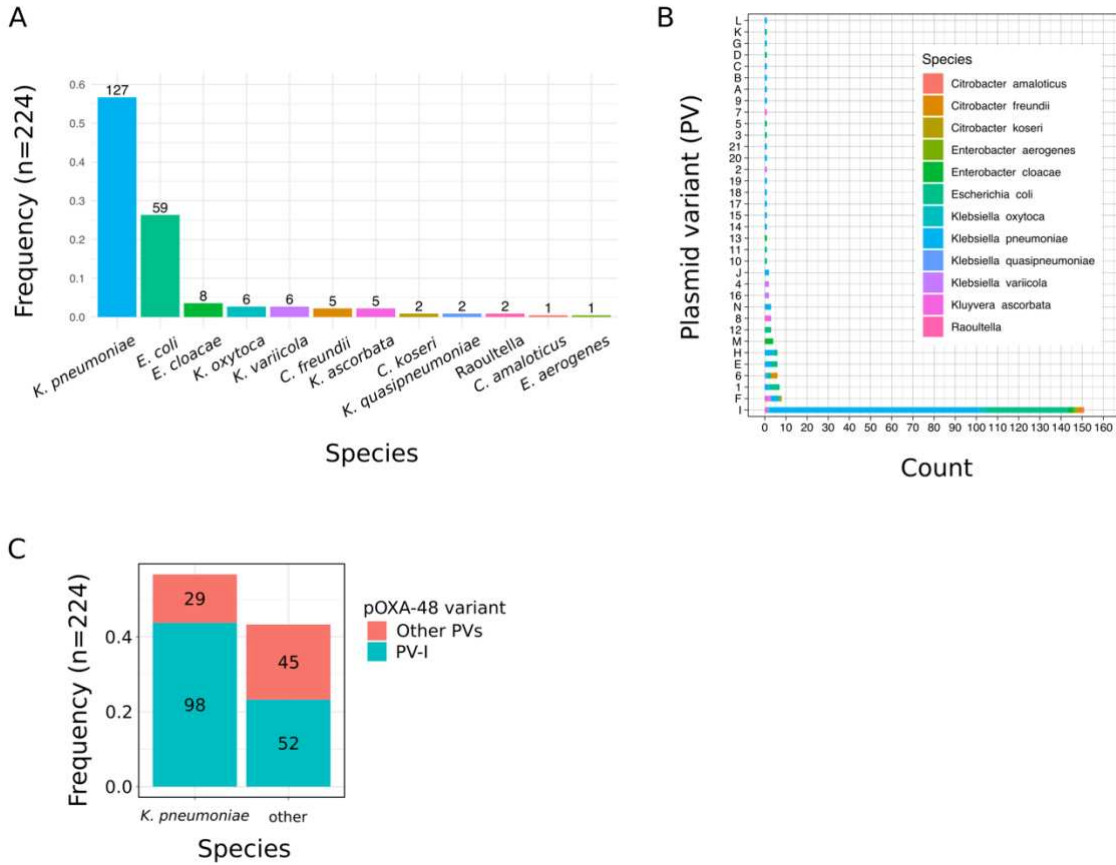
869 59. Letunic, I. & Bork, P. Interactive Tree Of Life (iTOL) v5: an online tool for
870 phylogenetic tree display and annotation. *Nucleic Acids Research* **49**, W293–
871 W296 (2021).

872

873

874 **Supplementary figures**

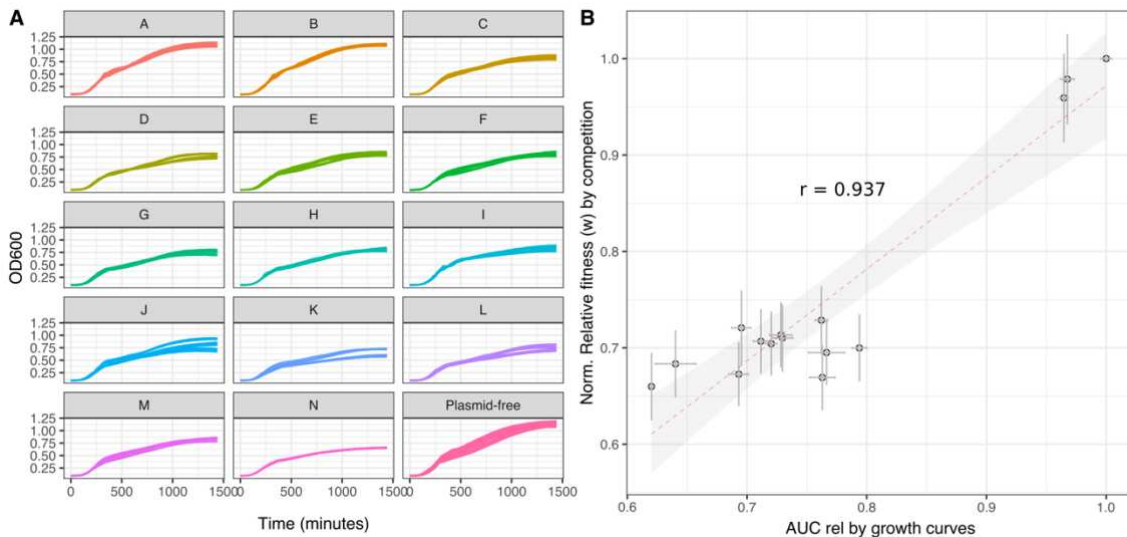
875



876

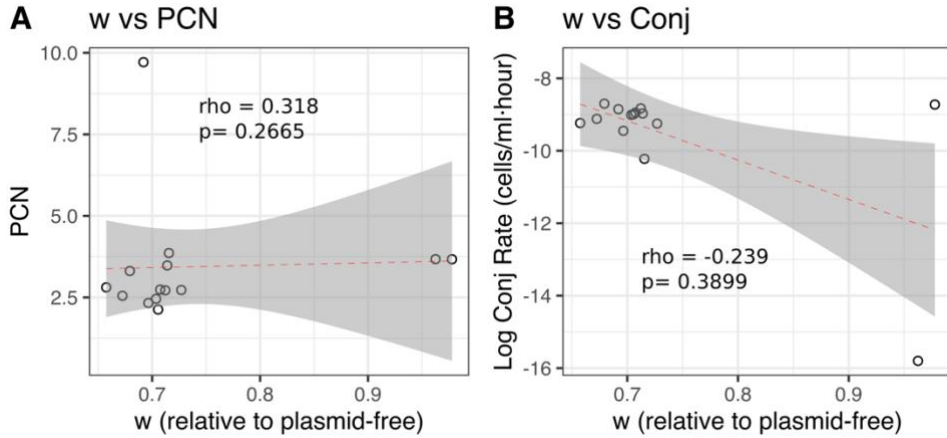
877 **Supp. Fig. 1 Enterobacteria carrying pOXA-48 recovered during the R-GNOSIS study. A)**

878 Frequency of clinical isolates by species. Numbers on top of the bars indicate the number of
879 isolates. B) Distribution of PVs from the collection by count and species (colours). C) Frequency
880 of isolates of *K. pneumoniae* or other enterobacteria carrying the most common pOXA-48 variant,
881 PV-I. Colours correspond to the PVs variant and the number within the bars correspond to the
882 isolate count.



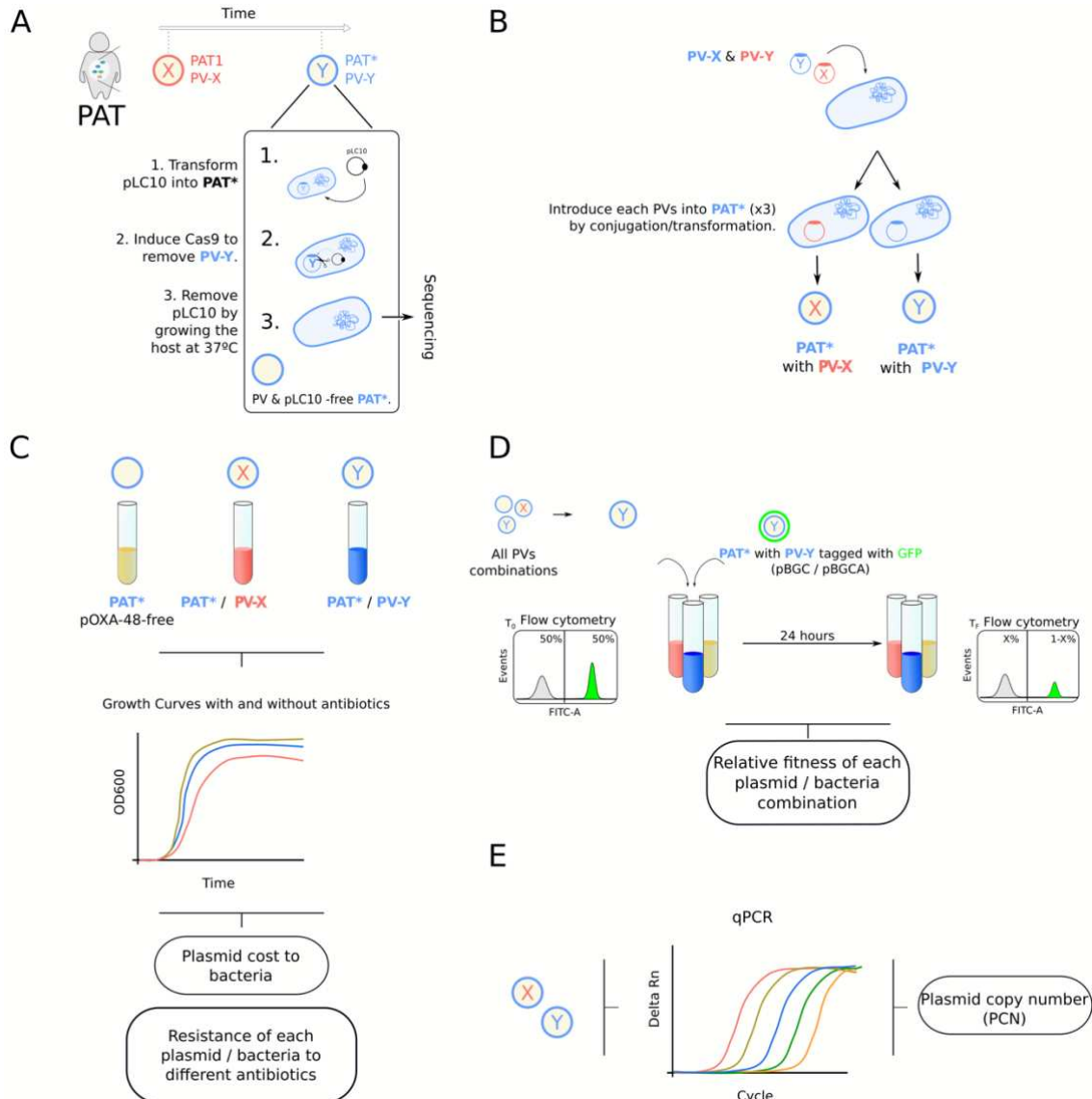
883

884 **Supp. Fig. 2 Growth dynamics of *E. coli* J53 carrying different PVs.** A) Growth curves of *E.*
885 *coli* J53 carrying different PVs. Vertical axis shows the optical density at 600 nm (OD600) and the
886 horizontal axis time in minutes. Each PV is indicated in the top label. B) Linear correlation of
887 relative fitness (w) calculated by competition assays or by area under the growth curves
888 (Pearson's product-moment correlation $t = 9.6665$, $df = 13$, $P = 2.663e-07$, $cor 0.9369456$). Lines
889 indicate the propagated standard error of the mean and points indicate the mean values for each
890 genotype.



891

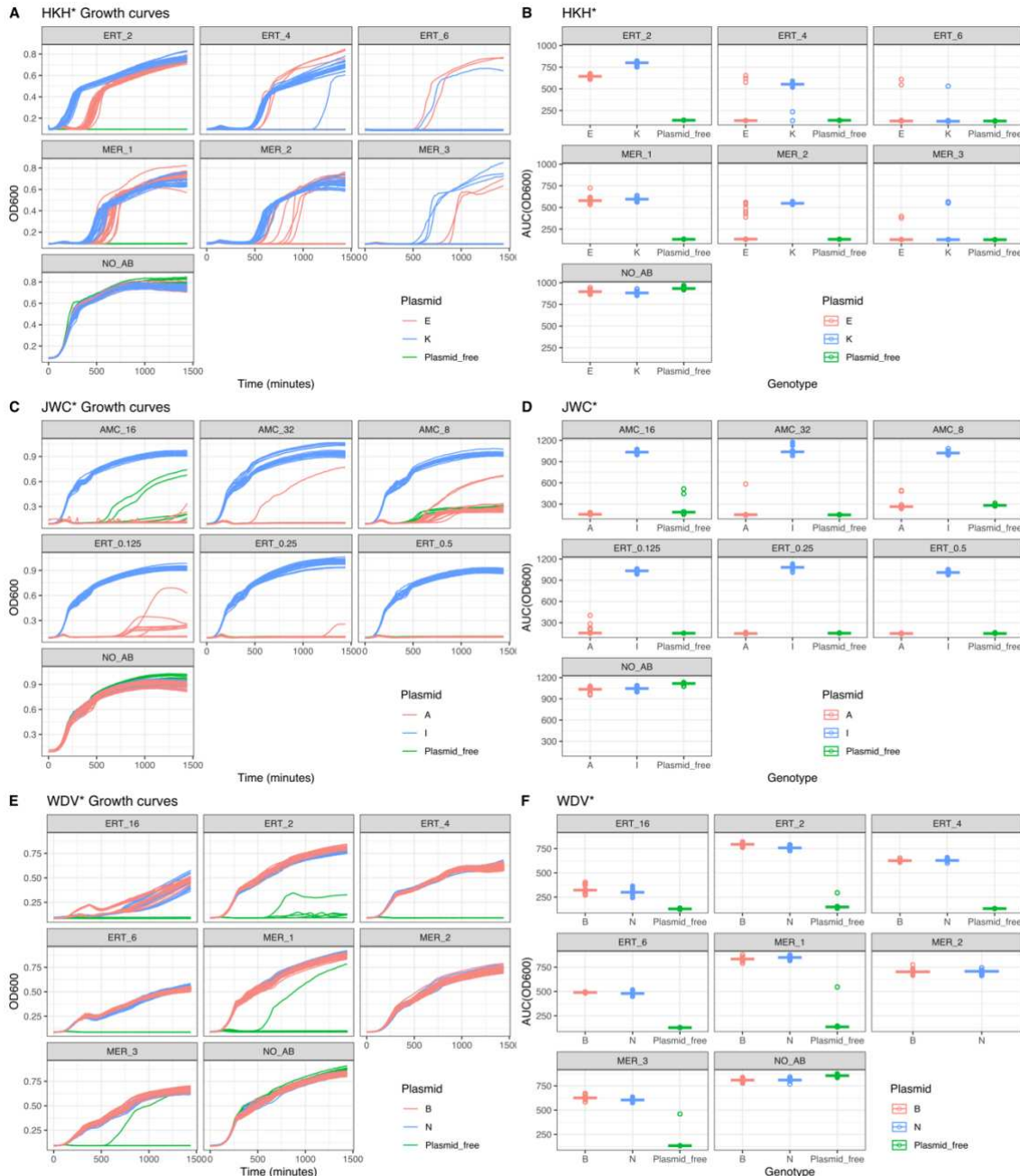
892 **Supp. Fig. 3 Plasmid copy number (PCN) and conjugation rates do not correlate with**
893 **plasmid fitness costs.** Correlation between relative fitness (w) and A) PCN, or B) \log_{10}
894 conjugation rate of *E. coli* J53 carrying different PVs relative to the plasmid-free strain. In each
895 panel individual dots correspond to the median values of *E. coli* J53 carrying different PVs.
896 Spearman's rank correlation rho and p-value (p) for each case are indicated in the figure.



897

898 **Supp. Fig 4 Workflow used to explore within-patient AMR evolution.** A) PVs curing from
 899 clinical isolates; B) re-introduction of different PVs into the clinical isolates; C) evaluation of the
 900 plasmid-cost and the resistance profile of each plasmid-carrying bacteria combination; D) relative
 901 fitness (w) calculation; and E) calculation of plasmid copy number (PCN) for each PV.

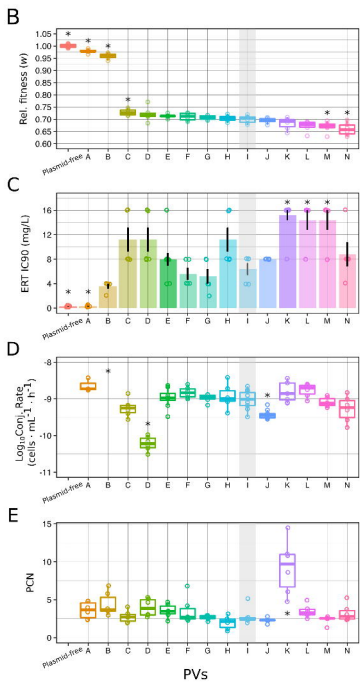
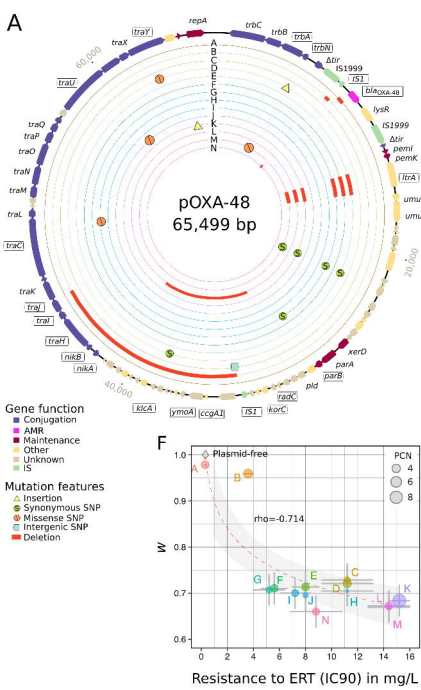
902



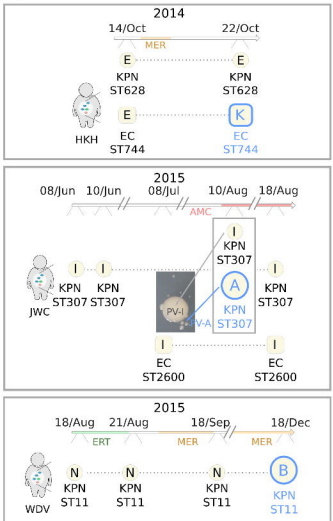
903

904 **Supp. Fig. 5 Growth dynamics of the clinical bacteria carrying different PVs isolated from**
 905 **the three patients under different antibiotic treatments.** A) Growth curves of HKH* carrying
 906 different PVs (indicated by different colours, see legend). Vertical axis shows the OD600 and
 907 horizontal axis the time in minutes. Each antibiotic concentration is indicated in the top label (ERT
 908 stands for ertapenem; MER for meropenem and NO_AB for no antibiotic treatment, the number
 909 indicates the concentration in mg/L). n=18 for each genotype and treatment. B) Growth of different
 910 HKH* carrying different PVs (as in A), using the values of the area under the curve (AUC in vertical
 911 axis, t = 1500 minutes). Individual points indicate individual values (n=18 for each genotype and
 912 treatment) and horizontal lines indicate the median value of the replicates. C) Growth curves of
 913 JWC* carrying different PVs (as in A). AMC stands for amoxicillin + clavulanic acid. D) Growth of
 914 different JWC* carrying different PVs using the values of the area under the curve (as in B). E)

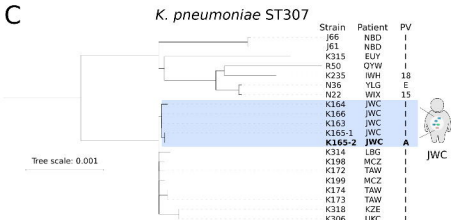
915 Growth curves of WDV* carrying different PVs (as in A and C). F) Growth of different WDV*
916 carrying different PVs using the values of the area under the curve (as in B and D).



A



C



D

Tree scale: 0.001

E. coli ST10 & ST744

Strain Patient PV ST

N46 BXD I ST10

C662 BXD I ST10

C166 YJX I ST10

C165 YJX I ST10

C289 HKH K ST744

C288 HKH E ST744

C718 DSO I ST10

C717 DSO I ST10

C643 JRV I ST10

C642 JRV I ST10

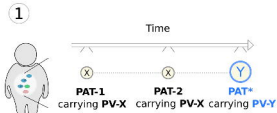
C667 OJZ I ST10

C646 HKO I ST10

C752 WIK I ST10

C728 CP I ST10

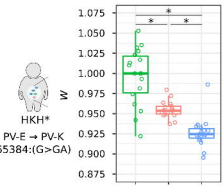
HKH

A

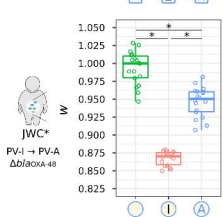
Isolation of potential cases of within-patient evolution

B

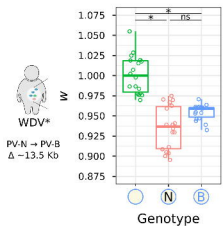
Relative fitness (*w*)



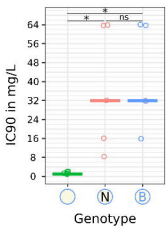
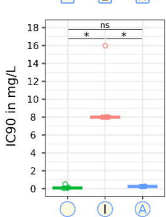
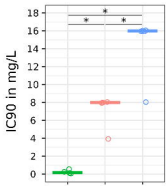
W



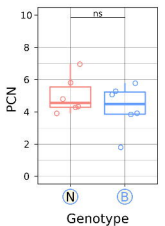
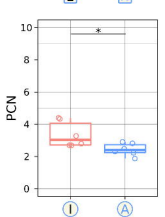
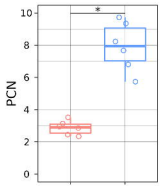
W

**C**

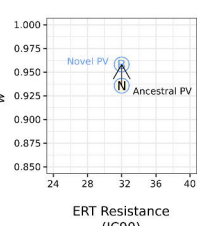
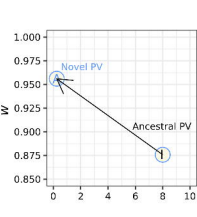
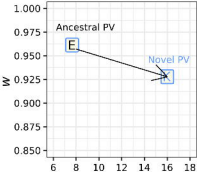
ERT Resistance

**D**

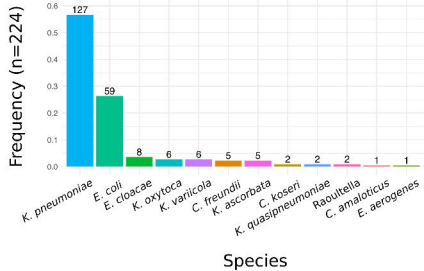
Plasmid copy number (PCN)

**E**

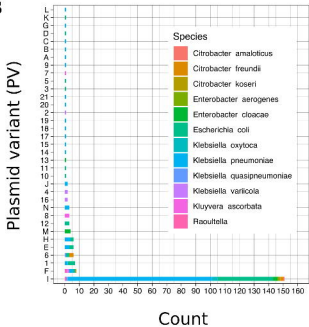
Trade-off fitness - resistance



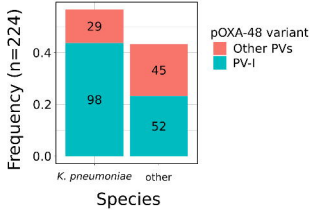
A

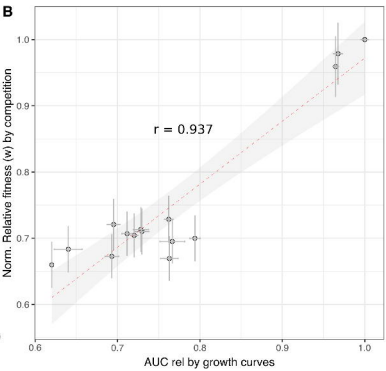
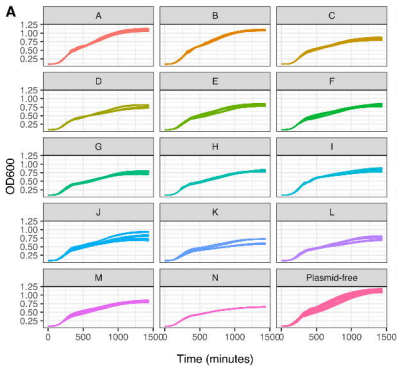


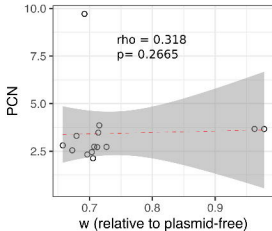
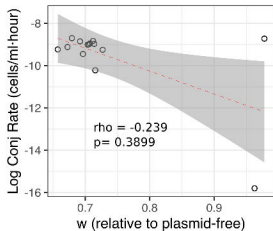
B



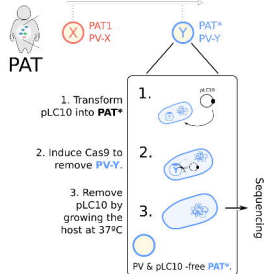
C



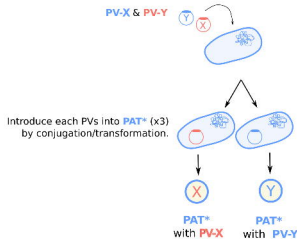


A w vs PCN**B** w vs Conj

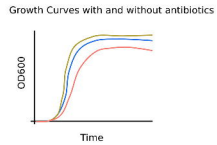
A



B



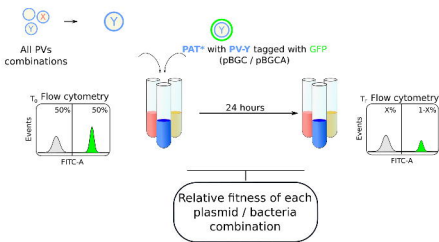
6



Plasmid cost to bacteria

Resistance of each plasmid / bacteria to different antibiotics

D



11

